AGU PUBLICATIONS

JGR

Journal of Geophysical Research: Space Physics

RESEARCH ARTICLE
10.1002/2014JA020383

Key Points:
- Cosmic dust significantly affects Earth's atmosphere
- Current estimates of cosmic dust influx vary by over 2 orders of magnitude
- Cosmic dust influx can be estimated from lidar measurements of Na flux

Correspondence to:
C. S. Gardner,
cgardner@illinois.edu

Citation:
Gardner, C. S., A. Z. Liu, D. R. Marsh, W. Feng, and J. M. C. Plane (2014), Inferring the global cosmic dust influx to the Earth's atmosphere from lidar observations of the vertical flux of mesospheric Na, *J. Geophys. Res. Space Physics*, *119*, doi:10.1002/2014JA020383.

Received 10 JUL 2014
Accepted 27 AUG 2014
Accepted article online 30 AUG 2014

Inferring the global cosmic dust influx to the Earth's atmosphere from lidar observations of the vertical flux of mesospheric Na

Chester S. Gardner[1], Alan Z. Liu[2], D. R. Marsh[3], Wuhu Feng[4], and J. M. C. Plane[4]

[1]Department of Electrical and Computer Engineering, University of Illinois at Urbana-Champaign, Urbana, Illinois, USA, [2]Department of Physical Sciences, Embry-Riddle Aeronautical University, Daytona Beach, Florida, USA, [3]Atmospheric Chemistry Division, National Center for Atmospheric Research, Boulder, Colorado, USA, [4]School of Chemistry, University of Leeds, Leeds, UK

Abstract Estimates of the global influx of cosmic dust are highly uncertain, ranging from 0.4–110 t/d. All meteoric debris that enters the Earth's atmosphere is eventually transported to the surface. The downward fluxes of meteoric metals like mesospheric Na and Fe, in the region below where they are vaporized and where the majority of these species are still in atomic form, are equal to their meteoric ablation influxes, which in turn, are proportional to the total cosmic dust influx. Doppler lidar measurements of mesospheric Na fluxes made throughout the year at the Starfire Optical Range, New Mexico, (35°N) are combined with the Whole Atmosphere Community Climate Model predictions of the relative geographic variations of the key wave-induced vertical transport processes to infer the global influxes of Na vapor and cosmic dust. The global mean Na influx is estimated to be 16,100 ± 3200 atoms/cm^2/s, which corresponds to 278 ± 54 kg/d for the global input of Na vapor and 60 ± 16 t/d for the global influx of cosmic dust.

1. Introduction

The Earth formed 4.5 billion years ago by accretion of debris from the solar nebula. Today Earth continues to accrete interplanetary dust particles whose global mass influx is estimated to be up to several hundred metric tons per day (t/d). Much of this incoming mass ablates—that is, the refractory metal-silicate constituents vaporize, as the high-speed particles undergo frictional heating due to collision with air molecules in the upper atmosphere [*Vondrak et al.*, 2008]. The main sources of cosmic dust are the sublimation of comets as they approach the Sun and collisions between asteroids in a belt between the orbits of Mars and Jupiter [*Janches et al.*, 2006; *Nesvorny et al.*, 2010, 2011]. Dust particles from long-decayed cometary trails, in particular from comets Encke and 55P/Temple-Tuttle, dominate the continuous sporadic input, while fresh dust trails, produced by comets that crossed the Earth's orbit within the past several hundred years, are the origin of meteor showers like Perseids.

The significant impact of cosmic dust on the Earth's atmosphere is only now beginning to be fully appreciated. Significant energy and substantial mass are deposited into the atmosphere by meteor deceleration, sputtering, and ablation between 80 and 120 km altitude. The meteoric debris is transported both downward, by gravity, advection, eddy mixing, and other wave effects, and poleward, by the meridional circulation system. The ablated atoms and the meteoric smoke particles (MSPs), which they eventually form through chemical reactions and condensation from the gas phase, are involved in a wide variety of atmospheric chemical processes [e.g., *Plane*, 2003], play important roles in the formation of mesospheric and stratospheric clouds [e.g., *Turco et al.*, 1981], and, when the iron-rich MSPs settle into the Southern Ocean around Antarctica, they fertilize the growth of phytoplankton, which impacts the atmospheric CO_2 cycle and potentially climate [*Petit et al.*, 1999; *Dhomse et al.*, 2013]. All of these effects obviously depend on the magnitude of the cosmic dust input.

Current estimates of the global influx of cosmic dust are highly uncertain, ranging from 0.4 to 110 t/d [*Nesvorny et al.*, 2011; *Plane*, 2012; *Langowski et al.*, 2014]. Spaceborne dust detection (e.g., microcrater observations on spacecraft surfaces) [*Love and Brownlee*, 1993] indicates a daily input of about 110 t, which is mostly in agreement with the accumulation rates of cosmic elements in polar ice cores [*Wasson and Kyte*, 1987; *Gabrielli et al.*, 2004; *Lanci and Kent*, 2006] and deep sea sediments [*Peucker-Ehrenbrink*, 1996]. In contrast, measurements of the products of meteoric ablation such as ionized meteor trails and meteoric

smoke particles in the middle atmosphere—by radar [*Mathews et al*., 2001; *Fentzke and Janches*, 2008], high-flying aircraft [*Cziczo et al*., 2001], and satellite remote sensing [*Hervig et al*., 2009]—and modeling of the meteoric metal layers [*Marsh et al*., 2013a; *Feng et al*., 2013; *Langowski et al*., 2014] indicate that the daily input is only 0.4–40 t.

In this paper, we derive a new estimate for the mean daily influx of cosmic dust by employing Doppler lidar measurements of the vertical flux of mesospheric Na atoms [*Gardner and Liu*, 2010] and the Whole Atmosphere Community Climate Model (WACCM) predictions of the relative geographic variations of the key vertical transport processes [*Marsh et al*., 2013b]. All of the meteoric debris that enters the atmosphere is eventually transported to the surface. Therefore, the influx of metals like Na and Fe can be determined by measuring the vertical fluxes of these species at altitudes below where they are injected into the atmosphere and where the majority of the species is still in atomic form. At the appropriate altitude, the global downward flux of a species is equal to its global meteoric influx. The cosmic dust influx is then estimated by scaling the measured species flux. To apply this technique, there are three important questions that need to be addressed (1) what fraction of the species in the cosmic dust particles vaporizes, (2) what fraction of the species flux is observed by the lidar, and (3) how is a vertical flux measurement made at a single site, or a small number of sites, scaled to obtain the global average?

2. Vaporization of Cosmic Dust

Vaporization of the cosmic dust involves several processes, which depend on the mass and velocity of the particles as well as the volatility of their constituents. These processes include sputtering by inelastic collisions with air molecules before the particle melts and diffusion-controlled migration of volatile constituents through the molten particle followed by evaporation of atoms and oxides from the melt. *Vondrak et al*. [2008] have studied these processes in considerable detail and developed a chemical ablation model (CABMOD) to predict the vaporization of specific constituents as a function of particle mass and speed. They have shown that the most volatile elements, like Na and K, evaporate rapidly even before the particle melts at around 1800 K. The main constituents Si, Fe, and Mg vaporize next, a few km lower, when the temperature increases above ~1850 K. Refractory elements like Ca, Al, and Ti ablate last at the lowest altitudes and hottest temperatures above ~2500 K. *Janches et al*. [2009] have observed this differential ablation using high-power meteor radars. *Vondrak et al*. [2008] computed the injection rate profiles for several elements and concluded that for reasonable cosmic dust mass and velocity distributions, the majority of Na and K vaporizes above 90 km altitude (see below).

Nesvorny et al. [2010, 2011] employed zodiacal cloud observations and model calculations to derive the distribution of meteoric debris accreted by the Earth for Jupiter-family cometary particles, which are believed to be a major source of cosmic dust entering the Earth's atmosphere. The debris mass falls into the four categories (1) sputtered mass, (2) ablated mass, (3) cosmic spherules (melted), and (4) unmelted micrometeorites. In addition to the evaporated Na in the sputtered and ablated mass, virtually all of the Na in the melted cosmic spherules evaporates because of rapid diffusion to the surface [*Vondrak et al*., 2008]. Meteor velocities range from a low value of 11.2 km/s for particles in the same orbit as the Earth (prograde orbit) to 72.5 km/s for particles in a retrograde orbit [*Baggaley*, 2002]. Because the *Nesvorny et al*. [2010, 2011] mean particle velocity is relatively slow (~12–14 km/s), CABMOD calculations place a lower limit of 60–70% on the amount of Na that is vaporized. In contrast, the velocity distribution based on high performance, large aperture radar observations of meteor head echos has a mean velocity around 30 km/s [*Janches et al*., 2008; *Pifko et al*., 2013]. For this faster distribution, CABMOD predicts that almost all of the Na vaporizes because a large fraction of the particles melt [*Marsh et al*., 2013a]. It has been shown that the radars used by Janches and coworkers to characterize the particle velocities are biased toward observing faster particles [*Janches et al*., 2008] and so the true velocity distribution is believed to be slower. In the present study we adopt a value of 0.925 for the Na ablation fraction, which was calculated by CABMOD using the particle mass and velocity distributions inferred from the Long Duration Exposure Facility (LDEF) observations [*Love and Brownlee*, 1993]. The mean velocity of the LDEF distribution is ~18 km/s, which implies that a significant fraction of the particles are in a prograde orbit.

The primitive CI carbonaceous chondrite meteors, which are most representative of the original solar nebula in composition, are composed of 0.5% Na by weight [*Lodders et al*., 2009]. This value is based largely on

analysis of the Orgueil meteorite, which is the most massive of the CI chondrite falls. However, the compositional differences among CI chondrites are very small, so this value should be highly representative [*Lodders et al*., 2009]. Assuming 92.5% of the Na is vaporized, the Na influx represents 92.5% × 0.5% = 0.46% of the total cosmic dust mass influx. Thus, a global average Na influx of 1000 Na atoms/cm^2/s corresponds to 17.3 kg/d for the global Na vapor input and 3.74 t/d for the global cosmic dust influx. Notice that the cosmic dust influx is inversely proportional to the Na ablation fraction and the Na meteoric mass abundance. Therefore, the dust influx that we determine below can simply be scaled to another velocity distribution or meteorite type.

The ablated Na atoms are transported downward to chemical sinks below ~85 km by advection, eddy diffusion, and wave effects. The primary chemical reservoir for Na is $NaHCO_3$, which is permanently removed from the atmosphere by condensation onto metal-silicate smoke particles (i.e., MSPs) [e.g., *Plane*, 2003, 2004]. In the region between about 85 and 90 km altitude the majority of the atmospheric Na is in atomic form [e.g., *Marsh et al*. 2013a, Figure 2]. Because most of the Na vapor is injected above 90 km, measurements of the vertical flux of atomic Na between 85 and 90 km should be approximately equal to the meteoric influx of Na vapor.

3. Vertical Transport of Atmospheric Constituents

In the mesopause region between 80 and 100 km altitude, the vertical transport of heat and constituents is dominated by gravity waves, tides, planetary waves, and turbulence [e.g., *Walterscheid*, 1981; *Walterscheid et al*., 1987; *Xu et al*., 2003; *Gardner and Liu*, 2010; *Zhu et al*., 2010]. By comparison, molecular diffusion is negligible. In this region, four processes contribute to vertical transport (1) advection associated with the meridional circulation system (downward in winter and upward in summer), (2) eddy mixing associated with turbulence produced by breaking waves, (3) dynamical transport caused by the net vertical displacement imparted by dissipating, nonbreaking waves, and (4) chemical transport which arises from the combined effects of wave perturbations and irreversible chemical loss and production which produces a net flux [*Gardner and Liu*, 2010]. All four mechanisms can produce substantial vertical fluxes of atmospheric constituents, which directly affect the chemistry and structure of the mesosphere and lower thermosphere.

The vertical flux of Na is defined as the expected value of the product of the vertical wind (w) and the Na density (ρ_{Na}) profiles and is composed of four terms,

$$\overline{w\rho_{Na}} = \overline{w\rho_{Na}}|_{Adv} + \overline{w\rho_{Na}}|_{Eddy} + \overline{w\rho_{Na}}|_{Dyn} + \overline{w\rho_{Na}}|_{Chem}, \quad (1)$$

where the overbar denotes the sample average. The advective flux component is equal to the product of the mean vertical drift velocity (w^*) caused by wave forcing of the meridional circulation and the mean Na density.

$$\overline{w\rho_{Na}}|_{Adv} = w^*\overline{\rho}_{Na}. \quad (2)$$

The eddy flux component is caused by turbulent mixing from regions of higher concentrations to lower concentrations and is given by [*Colegrove et al*., 1966]

$$\overline{w\rho_{Na}}|_{Eddy} = -k_{zz}\left(\frac{1}{H} + \frac{1}{\overline{T}}\frac{\partial\overline{T}}{\partial z} + \frac{1}{\overline{\rho}_{Na}}\frac{\partial\overline{\rho}_{Na}}{\partial z}\right)\overline{\rho}_{Na}, \quad (3)$$

where k_{zz} is the eddy diffusivity, H is the pressure scale height, and $\overline{T}$ is the mean temperature profile. The dynamical flux component is caused by dissipating waves and is proportional to the heat flux [*Gardner and Liu*, 2010]

$$\overline{w\rho_{Na}}|_{Dyn} = \frac{(g/R - \Gamma_{ad})}{(\Gamma_{ad} + \partial\overline{T}/\partial z)}\frac{\overline{w'T'}}{\overline{T}}\overline{\rho}_{Na}, \quad (4)$$

where $\Gamma_{ad} = 9.5$ K/km is the adiabatic lapse rate of dry air, $R = 287$ m^2/K/s^2 is the gas constant of the dry atmosphere, and $g = 9.5$ m/s^2 is the acceleration of gravity. $\overline{w'T'}$ is the heat flux which is defined as the sample mean of the product of the wave-induced vertical wind (w') and temperature fluctuations (T').

Waves contribute to chemically induced transport whenever there is a nonzero correlation between the species fluctuations and the fluctuations in its chemical sources and sinks. If the wave perturbations of the sources and sinks result in a net decrease (increase) of the species, the chemical flux is negative (positive) or

Table 1. Comparison of Na Flux Measurements at 87.5 km Altitude[a]

Site	Observation Period	Dynamical + Chemical Flux	Dynamical Flux	Chemical Flux
Table Mt., CO (40°N)	Aug–Sep (59 h)	−11,900 ± 3,000	−6,600 ± 1,400	−5,300 ± 3,300
SOR, NM (35°N)	Annual Mean (370 h)	−10,700 ± 1,500	−6,900 ± 2,200	−3,800 ± 2,700
Maui, HI (21°N)	Jan–May (100 h)	−8,000 ± 3,600	−7,000 ± 2,800	−1,000 ± 4,600
Cerro Pachon, Chile (30°S)	Mar (44 h)	−12,000 ± 5,300		
Weighted mean		−10,700 ± 1,200	−6,700 ± 1,100	−3,800 ± 1,900

[a]Flux Units: Na atoms/cm^2/s.

downward (upward). The chemical flux is proportional to the variance of the wave-induced temperature fluctuations $\overline{(T')^2}$ and for Na is given by

$$\overline{w\rho_{Na}}|_{Chem} = \frac{\left(\frac{\overline{Q'_{Na}\rho'_{Na}}}{\overline{\rho}_{Na}} + \frac{\overline{Q'_{Na}T'}}{\overline{T}}\right)}{\left(\frac{1}{H} + \frac{1}{\overline{T}}\frac{\partial\overline{T}}{\partial z} + \frac{1}{\overline{\rho}_{Na}}\frac{\partial\overline{\rho}_{Na}}{\partial z}\right)} = \frac{\gamma_{Na}\overline{(T')^2}}{\left(\Gamma_{ad} + \partial\overline{T}/\partial z\right)}\overline{\rho}_{Na}, \quad (5)$$

where $Q'_{Na} = P'_{Na} - L'_{Na}$ and γ_{Na} ($s^{-1}\,K^{-1}$) are related to the chemical production (P_{Na}) and loss (L_{Na}) of Na [*Walterscheid and Schubert*, 1989; *Gardner and Liu*, 2010].

Na and Fe Doppler lidars can potentially measure the dynamical, chemical, and eddy fluxes of these species, provided that the instrument resolution is sufficient to observe the small-scale wave and turbulence fluctuations and the signal levels are large enough that the photon noise is negligible [*Gardner and Yang*, 1998; *Gardner and Liu*, 2014]. Unfortunately, they cannot measure the advective fluxes because the vertical drift velocities are too small (<cm/s). The most extensive Na flux observations published to date were made at the Starfire Optical Range (SOR), New Mexico (35°N) [*Gardner and Liu*, 2010]. Because the data were processed with a vertical resolution of 500 m and a temporal resolution of 2.5 min, only the gravity wave fluctuations were observed and so the measurements include only the dynamical and chemical fluxes. At this site the Na flux is negative (downward) between 85 and 100 km and exhibits annual and semiannual variations. The peak flux occurs at 87.5 km altitude, and the annual mean value is −10,700 ± 1500 Na atoms/cm^2/s [see *Gardner and Liu*, 2010, Figure 2c and Table 2]. If this value were representative of the global mean influx of Na vapor, then the corresponding influx of cosmic dust would be 40 ± 5.6 t/d. However, this value is too small because the measured Na flux does not include the advective and eddy fluxes, the flux associated with the Na vapor injected below 87.5 km and the flux of Na bearing compounds, which the lidar cannot observe. Furthermore, wave activity varies geographically so that the vertical transport of Na above SOR is unlikely to be representative of the global average.

In Table 1 are tabulated the Na fluxes measured at 87.5 km at four sites between 30°S and 40°N. The lidars measured the sum of the dynamical and chemical fluxes and also the heat flux. The dynamical flux was computed from (4), using the measured heat flux and then subtracted from the total flux to derive the chemical flux. The observation periods and the number of hours of observations are listed in the table. In general, the uncertainty in the total flux measurement is smaller when the observed fluxes are averaged over longer periods of time [*Gardner and Liu*, 2010]. The measured total Na fluxes are statistically significant even though the uncertainties at individual sites are large. Obviously, the Table Mountain (40°N), SOR (35°N), and Cerro Pachón (30°S) total flux values are comparable. All three sites are located at midlatitudes near major mountain ranges where gravity wave activity and vertical transport are strong. The total Na flux is about 30% smaller at Maui (21°N) [*Liu and Gardner*, 2005], which may be a consequence of the weaker gravity wave activity at this low-latitude, mid-ocean site. However, because the observations cover different parts of the year and the differences among the four sites are not statistically significant, it is not possible to draw any definitive conclusions about the geographical variability of the fluxes from the data listed in Table 1.

We focus on the extensive SOR observations because they were made throughout the year and can be used to compute the annual mean fluxes. The observations at the other three sites, which correspond to only a few months, are likely to be biased by seasonal variations in wave transport. To estimate the advective and eddy fluxes at SOR, we use (2) and (3) and the w^* and k_{zz} values at the same altitude (87.5 km) provided by WACCM [*Marsh et al.*, 2013b]. In WACCM, w^* arises from mass continuity in which upwelling in one location

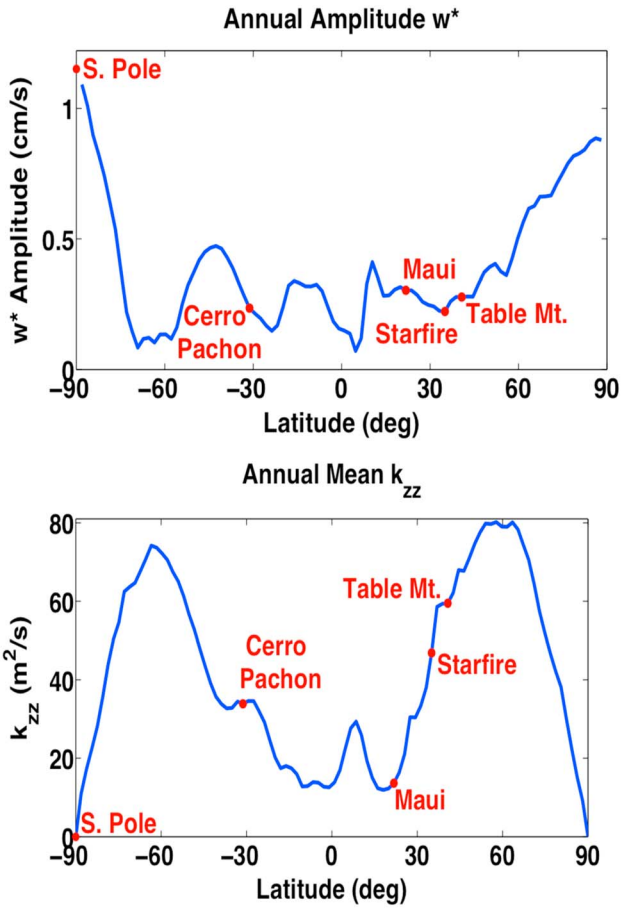

Figure 1. Latitudinal variations of (a) the annual amplitude of the zonal mean vertical drift velocity (w^*) at 87.5 km altitude and (b) the zonal and annual mean of the eddy diffusivity (k_{zz}) at 87.5 km altitude, both derived from WACCM simulations [*Marsh et al.*, 2013b].

is balanced by downwelling in another [*Andrews et al.*, 1987]. The eddy diffusivity k_{zz} is computed from a gravity wave parameterization scheme that is based upon a spectral model which includes waves excited in the atmosphere when stably stratified air flows over an irregular lower boundary and also by internal heating and shear [see *Garcia et al.*, 2007, Appendix]. The data for this study were obtained from WACCM for the period January 2010 to January 2013. The model was driven by Modern Era Reanalysis for Research and Applications as in *Marsh et al.* [2013a].

The vertical drift w^* is dominated by an annual oscillation with maximum upward velocity in midsummer. The zonal mean of the annual amplitude of w^* is plotted in Figure 1a. The velocity amplitude is typically much less than 0.5 cm/s between 60°S and 60°N, with values rising to about 1 cm/s near each pole. The mean of k_{zz} (zonal and annual average) is plotted in Figure 1b. The mean k_{zz} is maximum near 60° in both hemispheres reaching values between 75 and 80 m^2/s. At each pole k_{zz} is zero and less than 20 m^2/s near the equator. The four lidar sites are labeled in each figure. Notice that k_{zz} is more than twice as large at Cerro Pachón, SOR, and Table Mountain than it is at Maui.

Although WACCM does provide estimates of w^* and k_{zz} as a function of both latitude and longitude, on a seasonal timescale, the primary geographic variation of these parameters is latitudinal and so we employ the zonal mean values to estimate the advective and eddy fluxes at SOR. Estimates of the monthly mean advective fluxes were computed according to (2) by multiplying the monthly mean w^* values from WACCM, times the corresponding monthly mean Na densities measured by the SOR lidar. Estimates of the monthly mean eddy fluxes were derived according to (3) using the monthly mean k_{zz} values from WACCM and the monthly mean temperature and Na density profiles measured by the lidar. The annual mean Na fluxes are listed in Table 2. The mean advective flux is very small, while the eddy flux is comparable to the measured dynamical and chemical fluxes.

4. Global Average Na Flux and Cosmic Dust Influx

The total mean Na flux measured at 87.5 km altitude above SOR is $-16{,}700 \pm 1800$ Na atoms/cm^2/s. This value must be adjusted to account for the Na that is injected below 87.5 km and for the flux of Na bearing compounds at this altitude, which the lidar does not see. CABMOD calculations have shown that for fast particle distributions, such as the original *Fentzke and Janches* [2008] model, virtually all of the Na is injected above 90 km, while for the slowest particles a substantial amount of Na is injected below 90 km [e.g., see *Vondrak et al.*, 2008, Figures 10 and 11]. Based upon the CABMOD calculations for the LDEF velocity distribution, we find that 89% of the Na is injected above 87.5 km. Similarly, based upon the most current WACCM Na chemical model [*Marsh et al.*, 2013a], we find that 96% of the Na at 87.5 km is in atomic form.

Table 2. Annual Mean Vertical Fluxes of Atomic Na[a]

	Advective	Eddy	Dynamical	Chemical	Total
Annual mean measured at SOR (35°N)	−110	−5,900	−6,900	−3,800	−16,700 ± 1,800
Estimated global mean computed from (6)	−310	−5,610	−6,570	−3,620	−16,100 ± 3,200

[a]Flux Units: Na atoms/cm^2/s.

Therefore, the flux estimate derived from the lidar observations represents 89% × 96% = 85.44% of the total Na vapor influx at SOR.

The four flux components vary geographically because w^*, ρ_{Na}, k_{zz}, the heat flux, and the temperature variance all vary geographically. To determine the global mean, we need to scale the SOR data, taking into account the specific latitudinal variations of each of the four flux terms,

$$\overline{w\rho_{Na}}|_{GlobalMean} = \frac{\left(G_{Adv}\overline{w\rho_{Na}}|_{Adv} + G_{Eddy}\overline{w\rho_{Na}}|_{Eddy} + G_{Dyn}\overline{w\rho_{Na}}|_{Dyn} + G_{Chem}\overline{w\rho_{Na}}|_{Chem}\right)}{IF_{Na}OF_{Na}}$$
$$IF_{Na}(87.5\text{ km}) = \text{Injected Na Fraction Above 87.5 km}$$
$$OF_{Na}(87.5\text{ km}) = \text{Observed Na Fraction at 87.5 km}, \quad (6)$$

where G_x denotes the global mean scaling factor for the x flux component. For example, the global mean advective flux and scaling factor for SOR are given by

$$\overline{w^*\rho_{Na}}|_{GlobalMean} = \frac{\int_0^{360°+90°}\int_{-90°}\overline{w^*(\theta,\phi)\rho_{Na}(\theta,\phi)}\cos\theta\,d\theta\,d\phi}{\int_0^{360°+90°}\int_{-90°}\cos\theta\,d\theta\,d\phi} = \frac{1}{2}\int_{-90°}^{+90°}\overline{w^*(\theta)\rho_{Na}(\theta)}\cos\theta d\theta,$$
$$G_{Adv}(35°N) = \frac{\overline{w^*\rho_{Na}}|_{GlobalMean}}{\overline{w^*\rho_{Na}}|_{\theta=35°N}} = \frac{1}{2}\int_{-90°}^{+90°}\frac{\overline{w^*(\theta)\rho_{Na}(\theta)}}{\overline{w^*(35°N)\rho_{Na}(35°N)}}\cos\theta d\theta \quad (7)$$

where in this case the overbar denotes annual mean, which we assume is independent of longitude (ϕ).

The annual mean advective flux is negative, because w^* and ρ_{Na} both exhibit strong annual variations that are 180° out of phase. The flux is biased toward winter values because maximum downwelling occurs in midwinter when the Na density is also maximum. The seasonal variations in Na density are largely controlled by temperature. The Na density is maximum in midwinter when the mesopause region is warmest because the adiabatic heating associated with the downwelling is strongest. Consequently, the annual amplitude of ρ_{Na} is roughly proportional to the annual amplitude of w^*, and so the global distribution of the mean Na advective flux is approximately proportional to the square of the w^* annual amplitude. In this case the scale factor is given by

$$\overline{w^*(\theta)\rho_{Na}(\theta)} \propto -[w^*(\theta)]^2$$
$$G_{Adv}(35°N) = \frac{1}{2}\int_{-90°}^{+90°}\left[\frac{w^*(\theta)}{w^*(35°N)}\right]^2\cos\theta\,d\theta = 2.41, \quad (8)$$

where $w^*(\theta)$ denotes the amplitude distribution plotted in Figure 1a. The global mean advective flux of Na is approximately 2.41 times the SOR value.

Ground-based and satellite observations have shown that the annual mean Na layer structure does not vary significantly with latitude [e.g., *Fussen et al.*, 2010]. Therefore, we assume that the dominant geographical variation of the annual mean eddy flux is proportional to k_{zz} so that the scale factor is given by

$$G_{Eddy}(35°N) = \frac{1}{2}\int_{-90°}^{+90°}\frac{k_{zz}(\theta)}{k_{zz}(35°N)}\cos\theta\,d\theta = 0.813, \quad (9)$$

where $k_{zz}(\theta)$ denotes the distribution plotted in Figure 1b. According to the WACCM data, the global mean value of k_{zz} is 38 m^2/s at 87.5 km, and the value at SOR is 47 m^2/s. SOR is located in a region of higher than average wave activity, and so the SOR eddy flux is larger than the global average.

Unfortunately, the current gravity wave parameterization module in WACCM does not provide estimates of the heat flux or the temperature fluctuation variance. However, like k_{zz}, both of these parameters are directly related to the intensity of the gravity wave activity and wave dissipation. Large amplitude waves induce stronger temperature fluctuations and are more likely to experience dissipation, which increases the heat flux. These waves are also more prone to breaking, which generates turbulence and increases k_{zz} [e.g., *Zhao et al*., 2003]. Therefore, we use k_{zz} as a proxy for the geographic variations of both the dynamical flux, which is proportional to the heat flux, and the chemical flux, which is proportional to the temperature variance. If we assume the dynamical and chemical fluxes are proportional to k_{zz}, and then like the eddy flux, the global mean dynamical and chemical fluxes of Na are each about 81.3% of the values measured at SOR.

The global mean cosmic dust influx is computed by dividing the global Na flux by the fraction of Na that ablates and by the fraction of Na by weight in the dust particles (0.005)

$$\begin{aligned}
&\text{Global Cosmic Dust Influx} \\
&= \frac{-\left(G_{\text{Adv}}\overline{w\rho_{\text{Na}}}|_{\text{Adv}} + G_{\text{Eddy}}\overline{w\rho_{\text{Na}}}|_{\text{Eddy}} + G_{\text{Dyn}}\overline{w\rho_{\text{Na}}}|_{\text{Dyn}} + G_{\text{Chem}}\overline{w\rho_{\text{Na}}}|_{\text{Chem}}\right)}{0.005\text{AF}_{\text{Na}}\text{IF}_{\text{Na}}\text{OF}_{\text{Na}}} \\
&\text{G}_{\text{Adv}}(35°\text{N}) = \text{Advective Flux Global Scaling Factor at SOR} = 2.41 \\
&\text{G}_{\text{Eddy}}(35°\text{N}) = \text{Eddy Flux Global Scaling Factor at SOR} = 0.813 \\
&\text{G}_{\text{Dyn}}(35°\text{N}) = \text{Dynamical Flux Global Scaling Factor at SOR} = \text{G}_{\text{Eddy}}(35°\text{N}) = 0.813 \\
&\text{G}_{\text{Chem}}(35°\text{N}) = \text{Chemical Flux Global Scaling Factor at SOR} = \text{G}_{\text{Eddy}}(35°\text{N}) = 0.813 \\
&\text{AF}_{\text{Na}} = \text{Ablated Na Fraction} = 0.925 \text{ for LDEF dust model} \\
&\text{IF}_{\text{Na}}(87.5\text{ km}) = \text{Injected Na Fraction Above 87.5 km} = 0.89 \text{ for LDEF dust model} \\
&\text{OF}_{\text{Na}}(87.5\text{ km}) = \text{Observed Na Fraction at 87.5 km} = 0.96 \text{ for WACCM Na model}
\end{aligned} \tag{10}$$

By substituting the SOR flux values and scale factors into (6) and (10), the global mean Na influx is estimated to be 16,100 ± 3200 Na atoms/cm^2/s, which corresponds to 278 ± 54 kg/d for the global input of Na vapor and 60 ± 16 t/d for the global influx of cosmic dust. The uncertainties of these estimates cannot be determined precisely because the underlying uncertainties in some of the key parameters are either poorly known or difficult to estimate. However, realistic upper bounds on the uncertainties can be determined by making reasonable but conservative assumptions about the statistical characteristics of the parameters used to derive the global Na and cosmic dust influxes. The results of the error analysis are summarized in Table 3.

The eddy diffusivity in the mesopause region is difficult to measure and so there have been few observations of this important parameter. The most reliable data have been acquired using rocket-borne ionization gauge measurements of the neutral density fluctuations caused by turbulence. Because the rocket measurements are challenging and costly, the data are sparse. To our knowledge, the only site where enough measurements of k_{zz} have been made throughout the year to determine the annual mean value is Andøya, Norway (69°N) [*Lübken*, 1997]. The mean of the measured summer and winter k_{zz} values at 87.5 km for Andøya is 93 m^2/s. WACCM predicts 72 m^2/s for the zonal and annual mean at 69°N. The difference is about 22%. To be conservative, we assume that the RMS uncertainties in the WACCM k_{zz} values are ±30% with a temporal correlation period of 3 months and a latitudinal correlation length of 15°, which is roughly comparable to the scale of the latitudinal variations observed in Figure 1b. The accuracy of the calculated eddy flux at SOR (±16.9%) is dominated by the k_{zz} uncertainties, while the accuracy of the eddy flux global scaling factor is ±9.9% ($G_{\text{Eddy}} = 0.813 \pm 0.080$). The error contributions from the estimated SOR advective flux and global scaling factor are negligible because the advective flux is negligible. The accuracy of the measured dynamical plus chemical flux at SOR (±14%) is related to the number of hours of lidar observations [*Gardner and Liu*, 2010].

We assume that the RMS errors of the proxy function $k_{zz}(\theta)$, used to scale the dynamical (∝heat flux) and chemical (∝variance of temperature fluctuations) fluxes, are ±60% for both (i.e., twice the assumed k_{zz} error), with a latitudinal correlation length of 15°. The characteristics of these proxy errors are the least understood because of the lack of observational or model data. However, we believe our estimate of ±60% is conservative because, within the 1 standard deviation range, each proxy could vary by up to a factor of 4 at any latitude. This gives an RMS error of about ±19.8% for both scaling factors ($G_{\text{Dyn}} = 0.813 \pm 0.161$ and $G_{\text{Chem}} = 0.813 \pm 0.161$), which we assume are statistically independent.

Table 3. Error Analysis Summary

Parameter	Error Source	Parameter RMS Error	Global Na Vapor Influx RMS Error	Global Cosmic Dust Influx RMS Error
k_{zz}	WACCM	30%	NA	NA
SOR advective flux	Lidar + WACCM	-	Negligible	Negligible
SOR eddy flux	Lidar + WACCM	16.9%	16.4 kg/d	3.6 t/d
SOR Dyn + Chem flux	Lidar	14%	24.7 kg/d	5.3 t/d
Advective flux scaling $\propto (w^*)^2$	Lidar + WACCM	-	Negligible	Negligible
Eddy flux scaling $\propto k_{zz}$	WACCM $k_{zz}(\theta)$	9.9%	9.6 kg/d	2.0 t/d
Dyn flux scaling $\propto \overline{w'T'}$	WACCM $k_{zz}(\theta)$ Proxy	19.8%	22.5 kg/d	4.9 t/d
Chem flux scaling $\propto \left(T'\right)^2$	WACCM $k_{zz}(\theta)$ Proxy	19.8%	12.4 kg/d	2.6 t/d
Observed Na fraction	WACCM Na Chemical Model	4.2%	11.7 kg/d	2.5 t/d
Injected Na fraction	LDEF Particle Mass/Velocity Model CABMOD	12.4%	34.5 kg/d	-
Ablated Na fraction	LDEF Particle Mass/Velocity Model CABMOD	8.1%	NA	-
Injected × ablated Na fraction	LDEF Particle Mass/Velocity Model CABMOD	20.5%	NA	12.4 t/d
CI chondrite Na abundance	Orgueil meteorite inhomogeneities	5%	NA	3.0 t/d
Total RMS error			± 54.4 kg/d	± 15.6 t/d

Based upon the WACCM chemical model for mesospheric Na, we chose a value of 0.96 for the fraction of Na in atomic form at 87.5 km. For simplicity we assume that the 1 standard deviation confidence interval is symmetric about this value, which we estimate to be about ±4.2% so that $OF_{Na} = 0.96 \pm 0.04$. Based upon the CABMOD calculations for the LDEF particle velocity/mass distribution, we assume that the fraction of Na injected above 87.5 km is 0.89. This value decreases with decreasing particle velocities. We estimate the uncertainty to be ±12.4% so that $IF_{Na} = 0.89 \pm 0.11$. Finally, we chose a value of 0.925 for the Na ablation fraction, which is also consistent with CABMOD predictions for the moderately slow LDEF particle velocity distribution [*Vondrak et al*., 2008]. We estimate that the uncertainty in the assumed ablation fraction is about ±8.1% so that $AF_{Na} = 0.925 \pm 0.075$. Because the Na ablation and injection fractions both decrease with decreasing particle velocity, we assume the errors in these two parameters are correlated.

The WACCM Na model employs the faster *Janches et al*. [2008] velocity distribution model and a global mean Na vapor influx of just ~2000 Na atoms/cm^2/s, which is 8 times smaller than the value derived in this paper using the LDEF particle velocity model. Even so our results are valid because the WACCM dynamical parameters w^* and k_{zz} that are used to scale the SOR fluxes are derived from a gravity wave parameterization and are completely independent of the meteoric influx and particle velocity distribution. Furthermore, the fraction of Na in atomic form at 87.5 km (96%) is primarily a function of the chemical model used in WACCM and does not depend on the magnitude of the Na influx or the injection profile. Since Na is a minor constituent of the mesopause region, an increase (decrease) of the Na influx would result in a proportionate increase (decrease) in the densities of all the Na compounds, so that the fraction of atomic Na would be unchanged. In any event, other models of mesospheric Na, which were developed using much larger meteoric influx values than WACCM [e.g., *Plane*, 2004], also show that the majority of Na near 90 km altitude is in atomic form.

There are numerous analyses of Na in the Orgueil meteorite using modern mass spectrometry techniques. By eliminating those that deviate by more than 10% from the mean, *Lodders et al*. [2009] derived a mean of 4990 ppm for Na. Based upon the standard deviation of the values used to compute this mean, *Lodders et al*. [2009] estimated the accuracy to be ±250 ppm or about ±5%. The major source of this uncertainty is believed to be compositional inhomogeneities in the fine-grained structure of the meteorite.

5. Conclusions

Although numerous other techniques have been used to infer values for the daily cosmic dust influx that are both much larger and much smaller than the value reported here (see *Plane* [2012] for a summary), the lidar technique measures directly the downward flux of atomic Na right below the region of meteoric deposition. Hence, the flux measured by the lidar approximately equals the meteoric influx of Na vapor in the vicinity of the lidar site. Because the annual mean meteoric influx does not vary substantially geographically [*Marsh et al*., 2013a, Figure 1], the annual mean Na flux should not vary significantly with location either.

The average lifetime of a vaporized Na atom is approximately equal to the Na abundance (~4×10^9 Na atoms/cm^2/s) divided by the influx (~16,000 Na atoms/cm^2/s) or about 3 days. At mesopause heights the meridional winds average ~10 m/s toward the winter pole [see *Gardner and Liu*, 2007, Figure 2b]. Once a Na atom is vaporized at mesopause altitudes, it would be transported on average ~2500 km or ~22° in latitude before it is removed by chemistry. Thus, the Na flux measured at a single site is representative of the meteoric influx in the region within a few thousand km of the site. Existing measurements of the Na flux at four sites between 30°S and 40°N (Table 1), which are similar, support this conjecture. The mean of these measurements is −10,700 Na atoms/cm^2/s, which corresponds to a daily global Na influx of 185 kg. If a reasonable estimate for the eddy flux (−5000 Na atoms/cm^2/s) is added to the mean of the lidar measurements, the daily Na influx increases to about 270 kg. Thus, if 60% of the Na in the cosmic dust vaporizes (lower bound for the slowest particles), the cosmic dust influx would be 90 t/d, while if 100% vaporizes (upper bound for the fastest particles) the influx would be 54 t/d. This rough estimate demonstrates that the global influx must be at least many tens of metric tons per day. Our more sophisticated analysis, which is based upon the LDEF particle velocity and mass distributions, gives a value of 60 ± 15 t/d. We believe this value represents a lower bound. If the particle velocities are even slower than the LDEF model (~18 km/s) employed in our analysis, as *Nesvorny et al.* [2010, 2011] suggest (~12–14 km/s), then a smaller fraction of Na would evaporate, less Na would be injected above 87.5 km and as a consequence, the cosmic dust influx computed from (10) would increase.

The derived values for the Na and cosmic dust influxes reported here can be improved by directly measuring the Na eddy flux, in addition to the dynamical and chemical fluxes, by employing more powerful lidars with higher resolution sufficient to observe the turbulence fluctuations [*Gardner and Liu*, 2014]. In addition, measurements at multiple sites could be averaged to reduce the uncertainties and validate the scaling models used to calculate the global mean fluxes. Finally, observations of the Fe fluxes using Fe Doppler lidars would provide crucial information on differential ablation, which would be useful for validating and improving meteor ablation models like CABMOD and for refining estimates of the ablation and injection fractions. In fact, simultaneous observations of the Fe and Na fluxes can be used to constrain the particle velocity distribution since the ratio of the measured Fe to Na flux decreases with decreasing particle velocity as a smaller fraction of the Fe vaporizes compared to the more volatile Na.

Acknowledgments

This work was supported in part by National Science Foundation grants AGS 11-15725, AGS 11-15249, and AGS 11-15224. Liu's work was also partly supported by the National Natural Science Foundation of China through grant 41274151. The CABMOD modeling work was supported by the European Research Council (project number 291332-CODITA), and we thank Juan Diego Carrillo Sánchez for assistance with this. The authors also thank Xinzhao Chu and Wentao Huang at the University of Colorado-Boulder for providing the Table Mountain, CO observational data listed in Table 1. The data and programs used in this work are available upon request.

Alan Rodger thanks the reviewers for their assistance in evaluating this paper.

References

Andrews, D. G., J. R. Holton, and C. B. Leovy (1987), *Middle Atmosphere Dynamics*, Academic Press, San Diego, Calif.

Baggaley, W. J. (2002), Radar observations, in *Meteors in the Earth's Atmosphere*, edited by E. Murad and I. P. Williams, pp. 123–148, Cambridge Univ. Press, Cambridge, U. K.

Colegrove, F. D., F. S. Johnson, and W. B. Hanson (1966), Atmospheric composition in the lower thermosphere, *J. Geophys. Res.*, *71*(9), 2227–2236, doi:10.1029/JZ071i009p02227.

Cziczo, D. J., D. S. Thompson, and D. M. Murphy (2001), Ablation, flux and atmospheric implications of meteors inferred from stratospheric aerosol, *Science*, *291*, 1772–1775.

Dhomse, S. S., R. W. Saunders, W. Tian, M. P. Chipperfield, and J. M. C. Plane (2013), Plutonium-238 observations as a test of modeled transport and surface deposition of meteoric smoke particles, *Geophys. Res. Lett.*, *40*, 4454–4458, doi:10.1002/grl.50840.

Feng, W., D. R. Marsh, M. P. Chipperfield, D. Janches, J. Höffner, F. Yi, and J. M. C. Plane (2013), A global atmospheric model of meteoric iron, *J. Geophys. Res. Atmos.*, *118*, 9456–9474, doi:10.1002/jgrd.50708.

Fentzke, J. T., and D. Janches (2008), A semi-empirical model of the contribution from sporadic meteoroid sources on the meteor input function in the MLT observed at Arecibo, *J. Geophys. Res.*, *113*, A03304, doi:10.1029/2007JA012531.

Fussen, D., et al. (2010), A global climatology of the mesospheric sodium layer from GOMOS data during the 2002–2008 period, *Atmos. Chem. Phys.*, *10*, 9225–9236.

Gabrielli, P., et al. (2004), Meteoric smoke fallout over the Holocene epoch revealed by iridium and platinum in Greenland ice, *Nature*, *433*, 1011–1014, doi:10.1038/nature03137.

Garcia, R. R., D. R. Marsh, D. E. Kinnison, B. A. Boville, and F. Sassi (2007), Simulation of secular trends in the middle atmosphere, 1950–2003, *J. Geophys. Res.*, *112*, D09301, doi:10.1029/2006JD007485.

Gardner, C. S., and A. Z. Liu (2007), Seasonal variations of the vertical fluxes of heat and horizontal momentum in the mesopause region at Starfire Optical Range, New Mexico, *J. Geophys. Res.*, *112*, D09113, doi:10.1029/2005JD006179.

Gardner, C. S., and A. Z. Liu (2010), Wave-induced transport of atmospheric constituents and its effect on the mesospheric Na layer, *J. Geophys. Res.*, *115*, D20302, doi:10.1029/2010JD014140.

Gardner, C. S., and A. Z. Liu (2014), Measuring eddy heat, constituent and momentum fluxes with high-resolution Na and Fe Doppler lidars, *J. Geophys. Res. Atmos.*, *119*, doi:10.1002/2013JD021074.

Gardner, C. S., and W. Yang (1998), Measurements of the dynamical cooling rate associated with the vertical transport of heat by dissipating gravity waves in the mesopause region at the Starfire Optical Range, New Mexico, *J. Geophys. Res.*, *103*(D14), 16,909–16,926, doi:10.1029/98JD00683.

Hervig, M. E., L. L. Gordley, L. E. Deaver, D. E. Suskind, M. H. Stevens, J. M. Russell, S. M. Bailey, L. Megner, and C. G. Bardeen (2009), First satellite observations of meteoric smoke in the middle atmosphere, *Geophys. Res. Lett.*, *34*, L10803, doi:10.1029/2009GL039737.

Janches, D., C. J. Heinselman, J. L. Chau, A. Chandran, and R. Woodman (2006), Modeling the global micrometeor input function in the upper atmosphere observed by high power and large aperture radars, *J. Geophys. Res.*, *111*, A07317, doi:10.1029/2006JA011628.

Janches, D., S. Close, and J. T. Fentzke (2008), A comparison of detection sensitivity between ALTAIR and Arecibo meteor observations: Can high power and large aperture radars detect low velocity meteor head-echoes, *Icarus*, *193*(1), 105–111, doi:10.1016/j.icarus.2007.08.022.

Janches, D., L. P. Dyrud, S. L. Broadley, and J. M. C. Plane (2009), First observation of micrometeoroid differential ablation in the atmosphere, *Geophys. Res. Lett.*, *36*, L06101, doi:10.1029/2009GL037389.

Lanci, L., and D. V. Kent (2006), Meteoric smoke fallout revealed by superparamagnetism in Greenland ice, *Geophys. Res. Lett.*, *33*, L13308, doi:10.1029/2006GL026480.

Langowski, M., C. von Savigny, J. P. Burrows, W. Feng, J. M. C. Plane, D. R. Marsh, D. Janches, M. Sinnhuber, and A. C. Aikin (2014), Global investigation of the Mg atom and ion layers using SCIAMACHY/Envisat observations between 70 km and 150 km altitude and WACCM-Mg model results, *Atmos. Chem. Phys. Discuss.*, *14*, 1971–2019, doi:10.5194/acpd-14-1971-2014.

Liu, A. Z., and C. S. Gardner (2005), Vertical heat and constituent transport in the mesopause region by dissipating gravity waves at Maui, Hawaii (20.7°N), and Starfire Optical Range, New Mexico (35°N), *J. Geophys. Res.*, *110*, D09S13, doi:10.1029/2004JD004965.

Lodders, K., H. Palme, and H. P. Gail (2009), *Abundances of Elements in the Solar System*, Landolt Berstein New Ser., vol. VI/4B, chap. 4.4, edited by J. E. Trüper, pp. 560–630, Springer Verlag, Berlin, Heidelberg, New York.

Love, S. G., and D. E. Brownlee (1993), A direct measurement of the terrestrial mass accretion rate of cosmic dust, *Science*, *262*, 550–553.

Lübken, F.-J. (1997), Seasonal variation of turbulent energy dissipation rates at high latitudes as determined by in situ measurements of neutral density fluctuations, *J. Geophys. Res.*, *102*(D12), 13,441–13,456, doi:10.1029/97JD00853.

Marsh, D. R., D. Janches, W. Feng, and J. M. C. Plane (2013a), A global model of meteoric sodium, *J. Geophys. Res. Atmos.*, *118*, 11,442–11,452, doi:10.1002/jgrd.50870.

Marsh, D. R., M. Mills, D. Kinnison, J.-F. Lamarque, N. Calvo, and L. Polvani (2013b), Climate change from 1850 to 2005 simulated in CESM1 (WACCM), *J. Clim.*, *26*(19), 7372–7391, doi:10.1175/JCLI-D-12-00558.

Mathews, J. D., D. Janches, D. D. Meisel, and Q. H. Zhou (2001), The mircrometeoroid mass flux into the upper atmosphere: Arecibo results and a comparison with prior estimates, *Geophys. Res. Lett.*, *28*, 1929–1932, doi:10.1029/2000GL012621.

Nesvorny, D., P. Jenniskens, H. F. Levison, W. F. Bottke, D. Vokrouhlicky, and M. Gounelle (2010), Cometary origin of the zodiacal cloud and carbonaceous micrometeorites. Implications for hot debris disks, *Astrophys. J.*, *713*, 816–836, doi:10.1088/0004-637X/713/2/816.

Nesvorny, D., D. Janches, D. Vokrouhlicky, P. Pokorny, W. F. Bottke, and P. Jenniskens (2011), Dynamical model for the zodiacal cloud and sporadic meteors, *Astrophys. J.*, *743*, 129, doi:10.1088/0004-637X/743/2/129.

Petit, J. R., et al. (1999), Climate and atmospheric history of the past 420,000 years from the Vostok ice core, Antarctica, *Nature*, *399*, 429–436.

Peucker-Ehrenbrink, B. (1996), Accretion of extraterrestrial matter during the last 80 million years and its effect on marine osmium isotope record, *Geochim. Cosmochim. Acta*, *60*, 3187–3196.

Pifko, S., D. Janches, S. Close, J. J. Sparks, T. Nakamura, and D. Nesvorný (2013), The meteoroid input function and predictions of midlatitude meteor observations by the MU radar, *Icarus*, *223*, 444–459, doi:10.1016/j.icarus.2012.12.014.

Plane, J. M. C. (2003), Atmospheric chemistry of meteoric metals, *Chem. Rev.*, *103*, 4963–4984.

Plane, J. M. C. (2004), A time-resolved model of the mesospheric Na layer: Constraints on the meteor input function, *Atmos. Chem. Phys.*, *4*(3), 627–638, doi:10.5194/acp-4-627-2004.

Plane, J. M. C. (2012), Cosmic dust in the Earth's atmosphere, *Chem. Soc. Rev.*, *41*(19), 6507–6518, doi:10.1039/C2CS35132C.

Turco, R., O. Toon, P. Hamill, and R. Whitten (1981), Effects of meteoric debris on stratospheric aerosols and gases, *J. Geophys. Res.*, *86*(C2), 1113–1128, doi:10.1029/JC086iC02p01113.

Vondrak, T., J. M. C. Plane, S. Broadley, and D. Janches (2008), A chemical model of meteoric ablation, *Atmos. Chem. Phys.*, *8*(23), 7015–7031, doi:10.5194/qcp-8-7015-2008.

Walterscheid, R. L. (1981), Dynamical cooling induced by dissipating internal gravity waves, *Geophys. Res. Lett.*, *8*(11), 1235–1238, doi:10.1029/GL008i012p01235.

Walterscheid, R. L., and G. Schubert (1989), Gravity-wave fluxes of O_3 and OH at the nightside mesopause, *Geophys. Res. Lett.*, *16*(7), 719–722, doi:10.1029/GL016i007p00719.

Walterscheid, R. L., G. Schubert, and J. M. Straus (1987), A dynamical-chemical model of wave driven fluctuations in the OH nightglow, *J. Geophys. Res.*, *92*, 1241–1254, doi:10.1029/JA092iA02p01241.

Wasson, J. T., and F. T. Kyte (1987), Comment on the letter "On the influx of small comets into the Earth's atmosphere II: Interpretation", *Geophys. Res. Lett.*, *14*(7), 779–780, doi:10.1029/GL014i007p00779.

Xu, J., A. K. Smith, and R. Ma (2003), A numerical study of the effect of gravity-wave propagation on minor species distributions in the mesopause region, *J. Geophys. Res.*, *108*(D3), 4119, doi:10.1029/2001JD001570.

Zhao, Y., A. Z. Liu, and C. S. Gardner (2003), Measurements of atmospheric stability in the mesopause region at Starfire Optical Range, NM, *J. Atmos. Sol. Terr. Phys.*, *65*, 219–232.

Zhu, X., J. H. Yee, W. H. Swartz, and E. R. Talaat (2010), A spectral parameterization of drag, eddy diffusion, and wave heating for a three-dimensional flow induced by breaking gravity waves, *J. Atmos. Sci.*, *67*, 2520–2536, doi:10.1175/2010JAS3302.1.